

## Original Article

### Criteria for the Addition of Prone Imaging to Myocardial Perfusion SPECT for Inferior Wall

Short Title: Additional method of the prone imaging

Koji Nakaya,<sup>1,2,3</sup> Masahisa Onoguchi,<sup>1</sup> Yoshihiro Nishimura,<sup>3</sup> Keisuke Kiso,<sup>3</sup> Hideki Otsuka,<sup>4</sup> Yoshifumi Nouno,<sup>3</sup> Takayuki Shibutani,<sup>1</sup> Eisuke Yasuda,<sup>2</sup>

<sup>1</sup> Department of Quantum Medical Technology, Graduate School of Medical Science, Kanazawa University, Kodatsuno 5-11-80, Kanazawa, Ishikawa 920-0942, Japan

<sup>2</sup>Department of Radiological Technology, Faculty of Health Science, Suzuka University of Medical Science, 1001-1 Kishioka, Suzuka City, Mie 510-0293, Japan

<sup>3</sup>Department of Radiology and Nuclear Medicine, National Cerebral and Cardiovascular Center Hospital, 5-7-1 Fujishirodai, Suita, Osaka, 565-8565, Japan

<sup>4</sup>Department of Medical Imaging/Nuclear Medicine, Tokushima University Graduate School, 3-18-15, Kuramoto-cho, Tokushima 770-8503, Japan

Corresponding author: Masahisa Onoguchi

Department of Quantum Medical Technology, Graduate School of Medical Science,  
Kanazawa University, Kodatsuno 5-11-80, Kanazawa, Ishikawa 920-0942, Japan. E-  
mail: [onoguchi@staff.kanazawa-u.ac.jp](mailto:onoguchi@staff.kanazawa-u.ac.jp); Tel: +81-76-265-2526

This study has received ethical review of the National Cardiovascular Research Center.

Sources of funding: None

## Introduction

In case of myocardial perfusion single-photon emission computed tomography (SPECT) (hereafter termed MPS), decreased accumulation of radioisotopes in the inferior wall region secondary to attenuation artifacts from the diaphragm is often observed. We often do such an experience. Differentiation between ischemia and infarction of the inferior wall (right coronary artery [RCA] disease) may be difficult. In such cases, we add prone imaging after supine imaging because differentiation between RCA disease and attenuation artifacts is reportedly enabled by comparison of the two imaging findings [1-4].

Recently, attenuation correction has been performed using a SPECT device equipped with computed tomography (CT), making it possible to differentiate RCA disease and attenuation artifacts [5]. However, because prone imaging involves no CT radiation exposure and is low-cost, we evaluate the inferior wall with the addition of prone imaging only when ischemia or infarction of the inferior wall is suspected at the time at which the SPECT examination is requested.

However, if the decrease in  $^{201}\text{Tl}$ Thallium chloride ( $^{201}\text{Tl}$ ) accumulation for the inferior wall is observed in patients who have not undergone additional prone imaging,

difference between RCA disease and artifacts may be difficult. Moreover, many MPS procedures are performed per day. Because our institutions receive a high number of patients who undergo MPS, the addition of prone imaging to MPS in all cases would cause a serious decrease in the throughput. Ideally, we should add prone imaging only if we determine the presence of a threat due to either RCA disease or artifacts on a SPECT image obtained in the supine position in a patient under stress. In such cases, a diagnosis of inferior wall disease could be made without decreasing throughput. However, the appropriate conditions in which prone imaging should be added remain unclear.

Therefore, in this study, we aimed to establish a criteria that will enable us to decide whether prone imaging should be added. We evaluated the site (segment) at which RCA disease or attenuation artifacts from the diaphragm would likely appear after supine imaging under stress and determined the threshold of decreased accumulation at the same segment for the addition of prone imaging.

## **Materials and Methods**

### **Patients**

From February 1, 2013 to April 31, 2014, 34 patients with suspected RCA disease at the time of requested MPS examination underwent prone imaging. These 34 patients were divided into artifact group (Group A) and RCA disease group (Group B). Group B was diagnosed by stenosis rate in the RCA area of coronary angiography inspection (CAG). If there is more than 75% stenosis in RCA region, the patient was group B. The patient who did not enforce CAG was distributed by stenosis rate of RCA in the coronary CT or by left ventricular ejection fraction (LVEF) value in echo cardiology. If there is more than 75% stenosis in RCA region in the coronary CT, the patient was group B. Then if LVEF value by the echo cardiology is less than 55%, the patient was group B. In addition, group A was the patients who do not fit into those of the index.

This retrospective study was approved by the ethics committee at the National Cerebral and Cardiovascular Center.

### **Processing acquisition and conditions of MPS**

In this study, we used stress  $^{201}\text{Tl}$  myocardial perfusion SPECT images. We administered 111 MBq of  $^{201}\text{Tl}$  intravenously. The mixed patient data of patient with adenosine-stress and patient with ergometer-stress were used, and we obtained a stress SPECT image in

the supine and prone positions. In this case, there is no case that low level exercise on treadmill is added to adenosine-stress at the same time.

We used two BrightView detector-type gamma cameras (Philips, Amsterdam, Netherlands). To collect the data, we used a cardiac high-resolution collimator designed for the heart with two detectors positioned at a 90° angle. Supine imaging were scanned at 6-degree intervals over 180 degrees (50s/step, 12.5 min in total) using step-and-shoot mode. Then we added prone imaging, and prone imaging were scanned at 6-degree intervals over 180 degrees (15s/step, 3.75 min in total) using step-and-shoot mode. The conditions for filtering in SPECT image reconstruction included a matrix of 64 × 64, amplification of 1.85 times, and a pixel size of 2.72 mm. The maximum likelihood expectation maximization method was used for image reconstruction, a Butterworth (supine imaging: order, 10; cutoff frequency, 0.50 cycle/cm, prone imaging: order, 10; cutoff frequency, 0.37 cycle/cm) was used as the preprocessing filter, and a JETStream Workspace Auto SPECT+ (version 3.5; Philips, Amsterdam, Netherlands) was used for image processing. We did not perform attenuation or scatter correction.

### **Evaluation of percent uptake of supine and prone imaging**

We used a 20-segment polar map with quantitative perfusion SPECT software [6, 7] to evaluate the minor axis of the reconstituted SPECT images. Both group A and B were assessed, and 10 segments of the inferior hemisphere, which together corresponded to the inferior wall, were used to calculate the percent uptake (%uptake) of supine and prone imaging. In addition, the %uptake of supine and prone imaging was compared using the %uptake growth rate of 10 segments during prone imaging, as demonstrated by the following formula:

$$\text{Growth rate (\%)} = \frac{\% \text{Uptake of prone} - \% \text{Uptake of supine}}{\% \text{Uptake of supine}} \times 100 (\%) \quad (1)$$

In addition, we evaluated a segment with a high %uptake growth rate after prone imaging. We had a boundary line to the first high value of group B. A segment with a high %uptake growth rate was a segment of higher value than the boundary line in the group A. The breakdown of each segment number of the 20-segment polar map classification is shown in Figure 1.

### **Threshold of additional prone imaging**

As noted above, we found a segment of prone imaging exhibiting a high %uptake growth rate in the group A. We therefore compared the %uptake for supine imaging in these segments of the group A and B. Next, to decide whether to add prone imaging, we calculated the threshold of the %uptake (decrease in radioisotope accumulation) of supine imaging using the %uptake level of the supine images for group A and B (all 34 patients). The threshold was assumed to represent the mean +2 standard deviation (SD) of the %uptake.

### **Statistical analysis**

The significant difference test of %uptake between supine and prone imaging in each segment was used Wilcoxon signed-rank test. The significant difference test of %uptake growth rate and %uptake for supine imaging in a high %uptake growth rate segments between group A and B in each segment was used Mann-Whitney U test.

### **Results**

#### **Patient study**

We classified 34 patients in group A (20 patients) and B (14 patients). The patient information of group A and B was shown in Table 1. The age, sex, height, body weight, and body mass index were not seen in the significant difference between group A and B, respectively. Then the diabetes mellitus and hypertension of coronary risk factors were not seen in the significant difference between group A and B, respectively. However, group B was significantly higher in the hyperlipidemia and smoking history of coronary risk factors than group A, respectively (Hyperlipidemia;  $p < 0.01$ , Smoking history;  $p < 0.05$ ).

### **Evaluation of %uptake for supine and prone imaging**

Representative images in the supine and prone positions of the group A and B are shown in Figure 2. A decrease in radioisotope accumulation in the inferior wall was seen in the supine imaging of the group A and in the supine and prone imaging of the group B. Accumulation in the inferior wall was seen in the prone imaging of the group A.

The %uptake in the supine and prone positions of both groups in all 10 segments is shown in Figure 3. In all segments except for the 17 segment both group A and

B, %uptake of prone imaging showed a high value as compared to the % uptake of supine imaging. %uptake of prone imaging in the segment 3, 4, 5, 9, 10, 11, 15, 16, and 20 had increased significantly in group A (segment 11, 15, and 20;  $p < 0.01$ , segment 3, 4, 5, 9, 10, and 16;  $p < 0.001$ ). Then %uptake of prone imaging in the segment 3, 4, 5, and 10 had increased significantly in group B (segment 5 and 10;  $p < 0.05$ , segment 3 and 4;  $p < 0.01$ ).

The %uptake growth rates in the 10 segments in the prone imaging are summarized in Figure 4. In the prone imaging of the group A and B, %uptake growth rates was recognized in all segments except segment 17. Furthermore, %uptake growth rates of group A was higher than that of Group B. %uptake growth rates of Group A in the segment 3, 4, 5, 9, and 10 had increased significantly (segment 3, 5, and 10;  $p < 0.05$ , segment 4 and 9;  $p < 0.01$ ). In addition, the segment which was a highest value for %uptake growth rate was segment 4 in a group B, and a value was 21.5. This value was the boundary line, and the segments with high %uptake growth rates (i.e., more than the boundary lines) were segments 3, 4, 5, and 10 in the group A.

### **Threshold of additional prone imaging**

The %uptake in segments 3, 4, 5, and 10 in both groups in the supine imaging are

summarized in Figure 5. The %uptake in segments 3, 4, 5, and 10 in the group A was  $48.3\% \pm 7.1\%$ ,  $49.7\% \pm 5.6\%$ ,  $58.8\% \pm 5.6\%$ , and  $62.5\% \pm 6.7\%$ , respectively. The %uptake in segments 3, 4, 5, and 10 in the group B was  $49.4\% \pm 5.1\%$ ,  $48.2\% \pm 4.8\%$ ,  $59.6\% \pm 6.0\%$ , and  $59.5\% \pm 8.4\%$ , respectively. There were no significant differences in 3, 4, 5, and 10 segments of %uptake between the group A and B. In addition, the %uptake in these segments among all 34 patients in the supine imaging is shown in Figure 6. We adopted the mean + 2SD of the %uptake in the 34 cases (both group A and B) as the threshold because there were no significant differences in 3, 4, 5, and 10 segments of %uptake between the group A and B. The threshold of the supine imaging %uptake at which to add prone imaging was 62%, 61%, 71%, and 76% in segments 3, 4, 5, and 10, respectively. When we set the standard value of each segment in mean +2SD, this value becomes the value including % uptake of 34 cases (both group A and B). When we add prone to a patient of % uptake less than this standard value, it is thought that differentiation of the attenuation arch fact from diaphragm and the inferior wall CAD are possible.

## Discussion

In this study, we evaluated the segment at which RCA disease or attenuation artifacts from the diaphragm would likely appear during supine imaging under stress study. For each segment, we also determined the threshold of decreased radioisotope accumulation at which to add prone imaging. In this study, it is mixed  $^{201}\text{Tl}$  MPS images data of exercise and pharmaceutical stress. Uptake into the liver in MPS using technetium 99m methoxy isobutyl isonitrile ( $^{99\text{m}}\text{Tc}$ -SESTA MIBI) has caused the difference in the exercise and pharmaceutical stress [8]. It affects the MPS image, and both images are different. However, there is no paper comparing the effects of the liver in exercise and pharmaceutical stress using  $^{201}\text{Tl}$ , and %uptake of SPECT data due to the exercise and pharmaceutical stress was similar. Therefore, we investigated using  $^{201}\text{Tl}$  MPS images data of the exercise and pharmaceutical stress.

We have used  $^{201}\text{Tl}$  as radiotracer.  $^{201}\text{Tl}$  redistribution occurs as early as 20 minutes after the injection as well as 20 minutes after post stress injection. It is considered that there is no influence of redistribution because the total scan time of supine imaging and prone imaging is 16.25 minutes in this study (mid scan time is about 8 minutes). Therefore, even in prone imaging, it is considered that there is no influence of underestimation of the inferior wall due to redistribution.

In addition, MPS by  $^{201}\text{Tl}$  requires a larger exposure dose than  $^{99\text{m}}\text{Tc}$ -SESTA

MIBI and  $^{99m}\text{Tc}$ -tetrofosmin. Hence, there are many clinical and academic reports using  $^{99m}\text{Tc}$ -SESTA MIBI and  $^{99m}\text{Tc}$ -tetrofosmin. However,  $^{201}\text{Tl}$  has the advantage of being administered as a single dose for both stress and resting imaging. Many facilities in Japan thus use  $^{201}\text{Tl}$  to save on the need for more personnel.  $^{201}\text{Tl}$  has long been used for myocardial blood flow testing, and it is excellent in detecting ischemia and evaluating myocardial viability (viability). The clinical value in the diagnosis of coronary artery disease is considered to be equivalent between  $^{201}\text{Tl}$  and  $^{99m}\text{Tc}$  [9].  $^{201}\text{Tl}$  has a lot of evidence so far. We used  $^{201}\text{Tl}$  for this study because it is primarily used in our hospital.

In this study, the classification of the patients were classified it in artifacts and the RCA disease group by using the diagnostic results of CAG or coronary CT or echo cardiology. If originally, the classification of the patient should be performed only in the diagnostic result of the CAG. However, in the hospital, the cardiac first diagnostic study in the outpatient is MPS. It becomes the system which does not perform CAG when it is judged that flow of blood is normal or a little bit of decline in MPS. Thus, in the patients who did not performed CAG, we classified it in artifacts and the RCA disease group using a result of other inspection.

In both artifacts and the RCA disease group, the age, sex, height, body weight, body mass index, diabetes mellitus and hypertension were not seen in the significant

difference. However, Hyperlipidemia and smoking history were higher in the RCA disease group (Hyperlipidemia;  $p < 0.05$ , Smoking history;  $p < 0.01$ ). Therefore Coronary risk factors was higher in the group of diseases.

In all segments except for the 17 segment of the artifact group, %uptake of prone imaging showed a high value as compared to the %uptake of supine imaging. In addition, in segments 3, 4, 5, and 10 segment of the RCA disease group, %uptake of prone imaging showed a high value as compared to the % uptake of supine imaging. And there were some high value segment of the %uptake growth rates of the RCA disease group. We understand that we also receive the attenuation artifact from diaphragm in the RCA disease group.

In this study, the segment that it was easy to receive of the attenuation artifact from diaphragm was a segment 3, 4, 5, and 10. These segments were the segment of %uptake growth rate in the artifact group beyond the boundary line of most high growth rate (segment 4) in the RCA group. The setting of the segment that it is easy to receive of the attenuation artifact from diaphragm is proper because there is a significant difference in %uptake growth rate between artifacts and the RCA group in these segments.

Furthermore, we determined the threshold at which to add prone imaging by calculating the %uptake in the supine imaging of all 34 patients. Additional prone

imaging was carried out only for patients who showed decreased accumulation in the inferior wall by supine imaging. This threshold allowed us to immediately evaluate the decreased accumulation in the inferior wall, and we demonstrated an improvement in the ability to diagnose the pathology of the inferior wall. The evaluation for inferior wall was possible in all patients. Number of cases used was 34 cases. When number of cases increases, the reference value may change. When we set the standard value of each segment in mean +2SD, this value becomes the value including % uptake of 34 cases (an artifact group and disease group). When we add prone to a patient of %uptake less than this standard value, it is thought that differentiation of the attenuation artifact from diaphragm and the RCA disease are possible. Moreover, the construction of criteria for the addition of prone imaging can improve the quality of the inferior wall diagnosis without a reduction in throughput because we add the prone imaging to only patients with reduced accumulation in the inferior wall.

Although we suggested the threshold of %uptake of segment 3, 4, 5, and 10 in 20-segment classifications in this study, this segment is the same segment in the 17-segment classifications. Therefore, this threshold is also applicable for 17-segment classifications.

In addition, the Guner LA and others find out the appearance part of the

attenuation artifact from diaphragm [10]. And they mention it with usefulness of addition of prone imaging for all cases. However, the throughput decreases because this method is to add a prone imaging even for normal patient. Therefore, we set a standard to add prone imaging.

The attenuation artifact from the diaphragm received on the inferior wall can be differentiated by seeing the endsystolic wall thickening and cinemode images with quantitative gated SPECT software (QGS) in  $^{99m}\text{Tc}$ -SESTA MIBI or  $^{99m}\text{Tc}$ -tetrofosmin [11]. As mentioned above,  $^{201}\text{Tl}$  also has clinical value in the diagnosis of coronary artery disease, and it is still in current use. Therefore, inferior wall evaluation of prone imaging using  $^{201}\text{Tl}$  is useful research. In addition, because both of them are useful for evaluating the inferior wall, we would like to consider comparison of inferior wall evaluation between prone imaging and QGS in the future.

In addition, the imaging time differs between supine imaging and prone imaging. Because supine imaging needs to acquire basic information on myocardial blood flow, it is performed in the conventional imaging time (50 sec/step). On the other hand, prone imaging performs imaging with shortened time (15 sec/step) for the purpose of confirming attenuation artifacts from the diaphragm. Because the image pickup time differs as described above, there is a difference in the image configuration between

supine and prone imaging. Therefore, optimization processing is performed on the image using a noise reduction filter so that the image quality of prone imaging approaches the image quality of supine imaging. However, it is still undeniable that there is a difference in image quality. Considering the fact that  $^{201}\text{Tl}$  has an early redistribution time of 20 minutes, and we want to unify the imaging time of both imaging so as to finish imaging within 20 minutes in the future. In addition, this study is being studied using  $^{201}\text{Tl}$ , and it is also necessary to conduct research on  $^{99\text{m}}\text{Tc}$ -SESTA MIBI or  $^{99\text{m}}\text{Tc}$ -tetrofosmin. At the same time  $^{201}\text{Tl}$  having energy of 73 keV, it is not good Radio Isotope suitable for gamma camera energy unlike  $^{99\text{m}}\text{Tc}$ -SESTA MIBI or  $^{99\text{m}}\text{Tc}$ -tetrofosmin. In that case, one cannot reduce to 15 sec/step. Therefore the examination using the  $^{99\text{m}}\text{Tc}$ -SESTA MIBI or  $^{99\text{m}}\text{Tc}$ -tetrofosmin must image in the same time interval of minimum 50 sec/step in supine as well as prone position.

Prone imaging is not affected by attenuation artifact from the diaphragm. Attenuation artifact may reportedly be observed along the imaging table because a detector collects it passing through the bottom of the imaging table [12]. To decrease attenuation artifact, an imaging table containing a cut-out section under the cardiac area for prone imaging was developed [13]. Adoption of this technique allowed for generation of a prone image with higher accuracy. The time required for prone imaging at our center

was 3 minutes 45 seconds, but maintenance of the prone position may be a physical burden for patients even during this short collection time. We wish to develop an imaging table that places less stress on patients in the prone position.

Development of a system that uses a prone image of the inferior wall in combination with supine images was recently reported [14], and the analysis of prone imaging has progressed. Moreover, coronary angiography in the prone position is an important diagnostic option for the detection of ischemia in patients with obstructive coronary artery disease [15]. This imaging method is effective for assessment of the inferior wall and should be considered for evaluating other abnormalities of the inferior wall.

In addition, recently it has advanced myocardial imaging device using the semiconductor detector. This device has been performed sitting position imaging. In obese patients, MPS should be performed by adding an upright image because MPS is insufficient in the supine position only [16]. We plan to compare prone and upright images in future studies.

## **Conclusion**

We constructed evaluation criteria to decide whether to add prone imaging for patients with decreased radioisotope accumulation in the inferior wall on supine imaging. Either inferior wall disease or attenuation artifact from the diaphragm is supposed to have caused the decreased %uptake in segments 3, 4, 5, and 10 of the supine images in the present study. These are indices for additional prone imaging, the performance of which is expected to improve the diagnosis of RCA disease.

### **Acknowledgement**

The authors acknowledge the staffs in National Cerebral and Cardiovascular Center in preparing the manuscript.

### **Sources of Funding**

None

### **Conflicts of Interest**

The authors have no potential conflicts of interest to disclose.

## References

- [1] Esquerre JP, Coca FJ, Martinez SJ, Guiraud RF. Prone decubitus: a solution to inferior wall attenuation in thallium-201 myocardial tomography. *J Nucl Med* 1989;30(3):398-401.
- [2] Segall GM, Davis MJ, Golis ML. Improved specificity of prone versus supine thallium SPECT imaging. *Clin Nucl Med* 1988;13(12):915-6.
- [3] Segall GM, Davis MJ. Prone versus supine thallium myocardial SPECT: a method to decrease artifactual inferior wall defects. *J Nucl Med* 1989;30(4):548-55.
- [4] Katayama T, Ogata N, Tsuruya Y. Diagnostic accuracy of supine and prone thallium-201 stress myocardial perfusion single-photon emission computed tomography to detect coronary artery disease in inferior wall of left ventricle. *Ann Nucl Med* 2008;22(4):317-21.
- [5] Fricke E, Fricke H, Weise R, Kammeier A, Hagedorn R, Lotz N. Attenuation correction of myocardial SPECT perfusion images with low-dose CT: evaluation of the method by comparison with perfusion PET. *J Nucl Med* 2005;46(5):736-44.
- [6] Germano G, Kavanagh PB, Waechter P, Areeda J, Van Krieking S, Sharir T. A

new algorithm for the quantitation of myocardial perfusion SPECT. I: Technical principle and reproducibility. J Nucl Med 2000;41(4):712-9.

[7] Sharir T, Germano G, Waechter PB, Kavanagh PB, Areeda JS, Gerlach J. A new algorithm for the quantitation of myocardial perfusion SPECT. II: Validation and diagnostic yield. J Nucl Med 2000;41(4):720-7.

[8] Primeau M, Taillerfer R, Essiambre R, Lambert R, Honos G. Technetium 99m SESTAMIBI myocardial perfusion imaging: comparison between treadmill, dipyridamole and trans-oesophageal atrial pacing "stress" tests in normal subjects. Eur J Nucl Med 1991;18(4):247-51.

[9] The Japanese Circulation Society. Guidelines for Clinical Use of Cardiac Nuclear Medicine. JCS 2010

[10] Guner LA, Caliskan B, Isik I, Aksoy T, Vardareli E, Parspur A. Evaluating the Role of Routine Prone Acquisition on Visual Evaluation of SPECT Images. J Nucl Med Technol. 2015 Dec;43(4):282-8.

[11] Germano G, Kiat H, Kavanagh PB, Moriel M, Mazzanti M, Su HT, Van Train KF, Berman DS. Automatic quantification of ejection fraction from gated myocardial perfusion SPECT. J Nucl Med 1995;36(11):2138-47.

[12] O'Connor MK, Bothun ED. Effects of tomographic table attenuation on prone and supine cardiac imaging. J Nucl Med 1995;36(6):1102-6.

[13] Kiat H, Van Train KF, Friedman JD, Germano G, Silagan G, Wang FP.

Quantitative stress-redistribution thallium-201 SPECT using prone imaging:

methodologic development and validation. *J Nucl Med* 1992;33(8):1509-15.

[14] Nishina H, Slomka PJ, Avidov A, Yoda S, Akincioglu C, Kang X. Combined

supine and prone quantitative myocardial perfusion SPECT: method development and

clinical validation in patients with no known coronary artery disease. *J Nucl Med*

2006;47(1):51-8.

[15] Shin JH, Pokharna HK, Williams KA, Mehta R, Ward RP. SPECT myocardial

perfusion imaging with prone-only acquisitions: correlation with coronary angiography.

*J Nucl Cardiol* 2009;16(4):590-6.

[16] Ben-Haim S, Almukhailed O, Neill J, Slomka P, Allie R, Shiti D. Clinical value of

supine and upright myocardial perfusion imaging in obese patients using the D-SPECT

camera. *J Nucl Cardiol* 2014;21(3):478-85.

**Figure legends**

**Fig. 1** Twenty-segment myocardial model

**Fig. 2** Comparison between supine and prone SPECT imaging under stress. The left image is the supine image, and the right image is the prone image. The left column shows the SPECT polar map, the middle column shows the SPECT short-axis image, and the right column shows the SPECT vertical-long image. (a) Attenuation artifact images. (b) Right coronary artery (RCA) disease images.

Patient (a) information: Age; 76, Sex; male, Height (cm); 166.8, Body weight (kg); 75.6, Body mass index; 27.2. Patient (b) information: Age; 70, Sex; male, Height (cm); 161.0, Body weight (kg); 67.3, Body mass index; 26.0

**Fig. 3**  $^{201}\text{Tl}$  chloride %uptake on myocardial perfusion SPECT under stress in 10 segments of the lower hemisphere. (a) Supine and prone imaging in the artifact group (group A). (b) Supine imaging in the right coronary artery (RCA) disease group (group B)

**Fig. 4**  $^{201}\text{Tl}$  chloride %uptake growth rate of 10 segments in prone imaging (the black line is the boundary line of the value of the segment 4 in the right coronary artery (RCA) disease group (group B), and the triangle indicates the segment in which the

growth rate is higher than the boundary line)

**Fig. 5** Comparison of supine %uptake in the artifact group (group A) and right coronary artery (RCA) disease group (group B) under stress. (a) Segment 3. (b) Segment 4. (c) Segment 5. (d) Segment 10

**Fig. 6** <sup>201</sup>Thallium chloride %uptake in the supine imaging of all 34 patients (the black line is the mean +2 standard deviation (SD) of the %uptake in 34 patients). If the %uptake is lower than the black line in four segments, we add prone imaging. (a) Segment 3. (b) Segment 4. (c) Segment 5. (d) Segment 10

### **Table legends**

**Table.1** Clinical characteristics of 34 patients

Fig.1

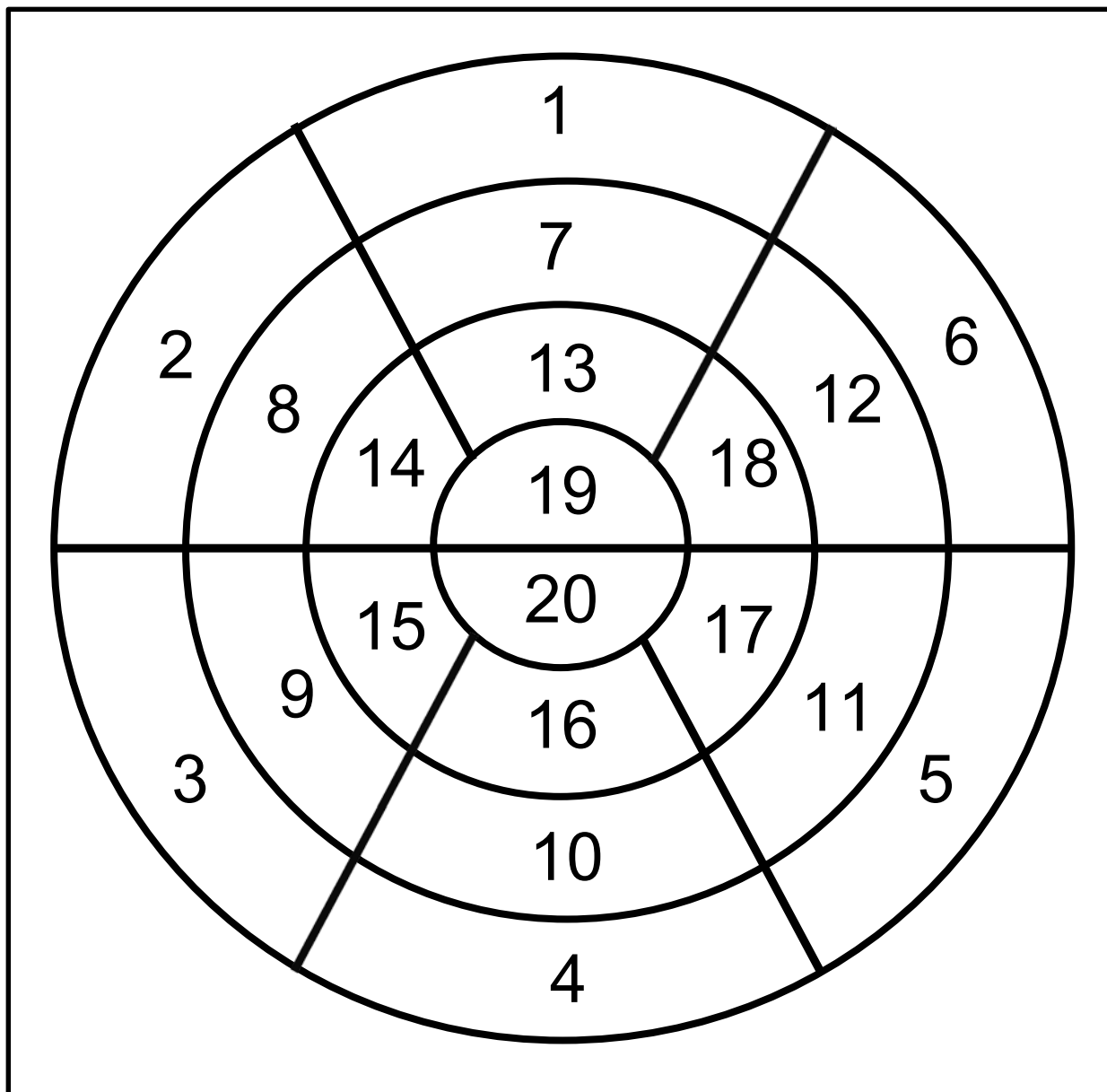


Fig.2

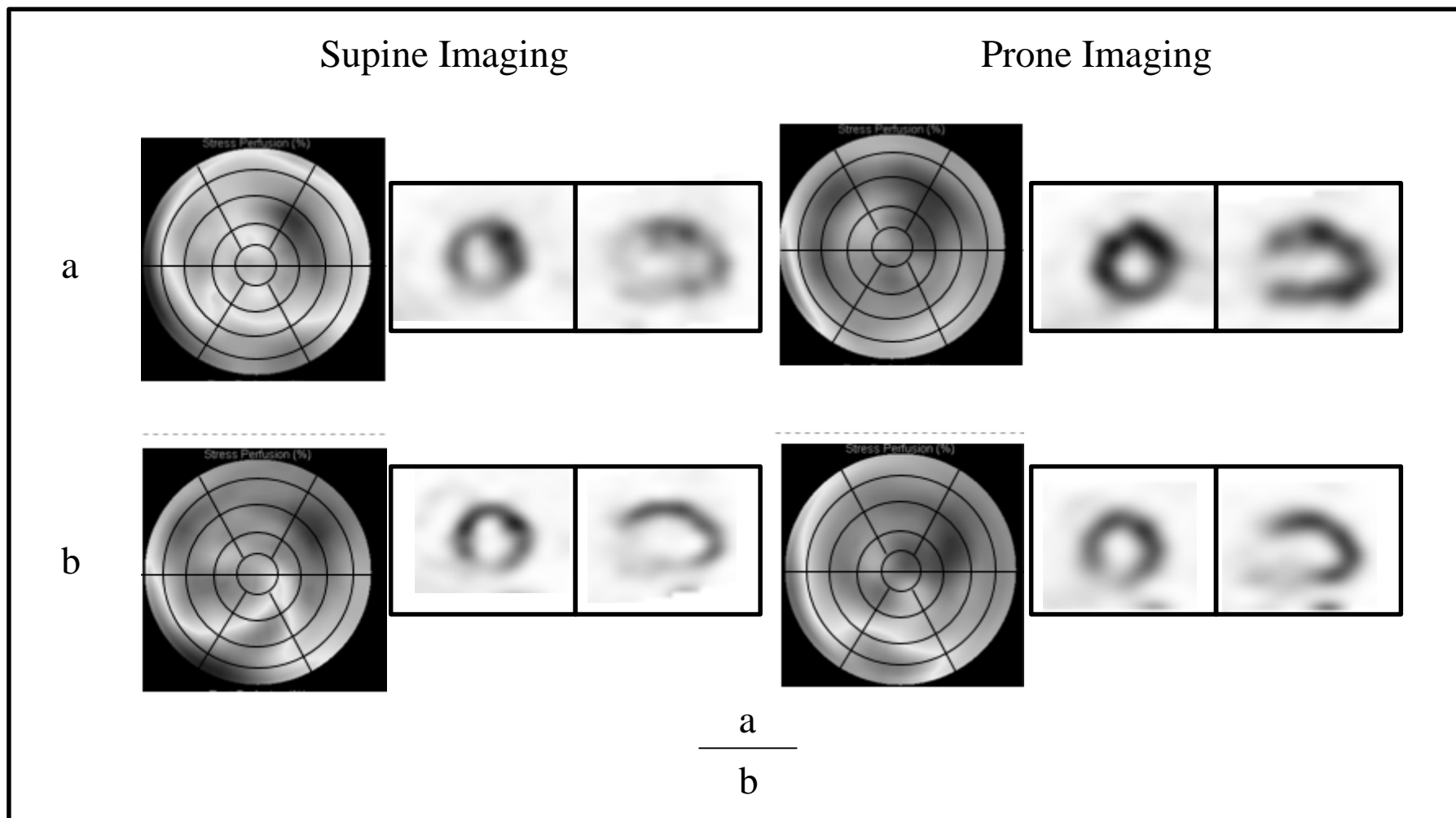
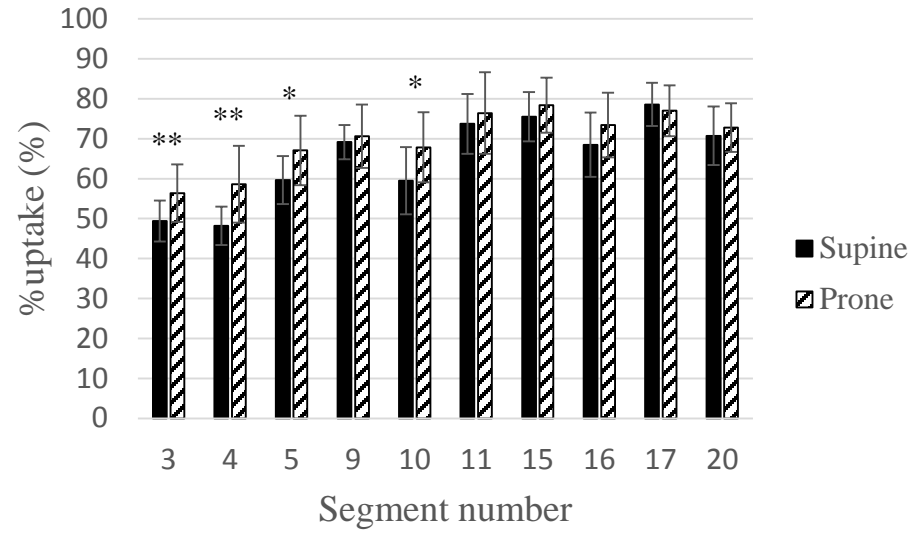
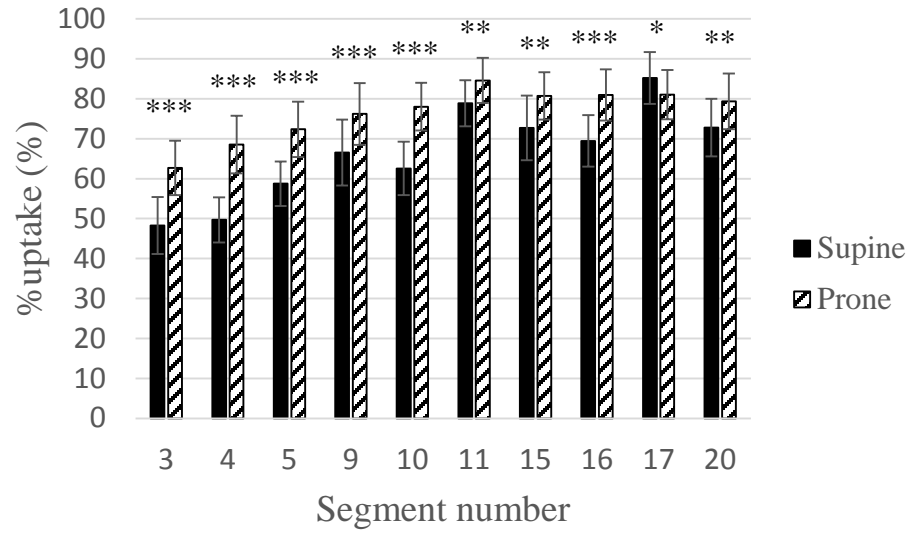


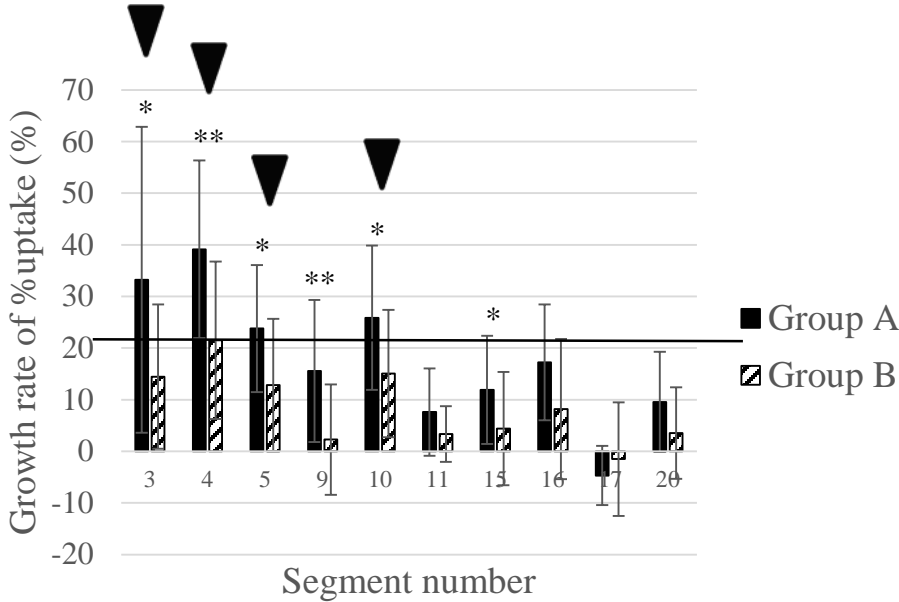
Fig.3



\*:  $p < 0.05$ , \*\*:  $p < 0.01$ , \*\*\*:  $p < 0.001$

a | b

Fig.4



\*: p<0.05, \*\*: p<0.01

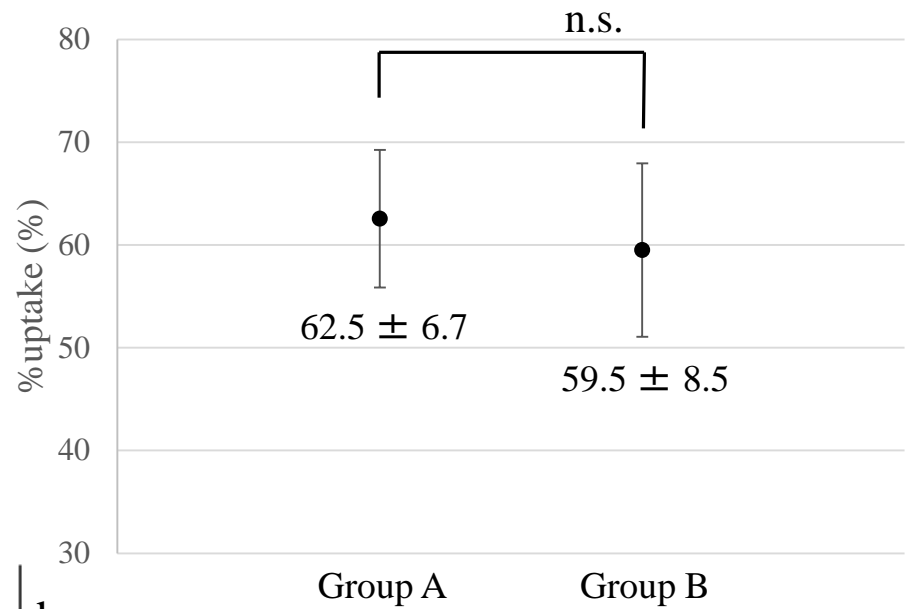
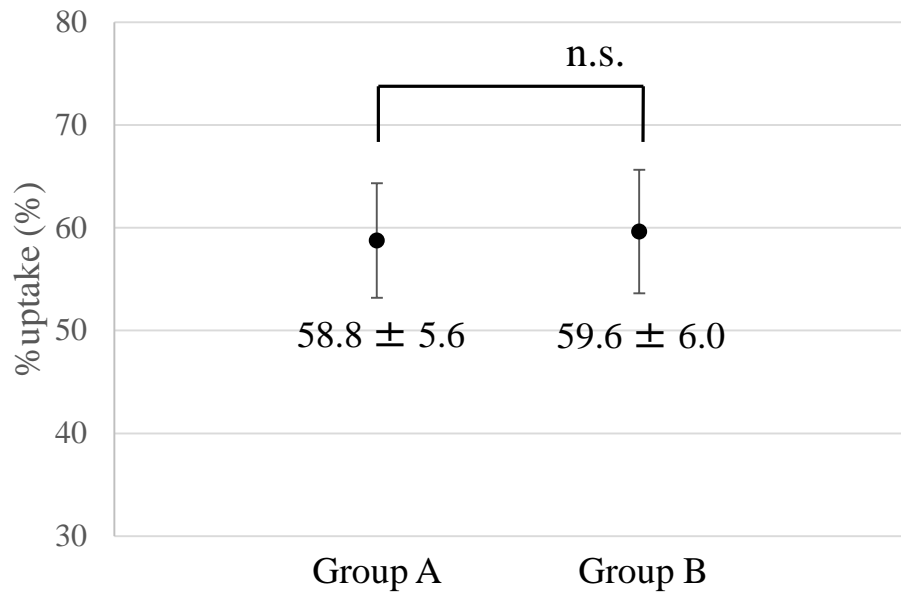
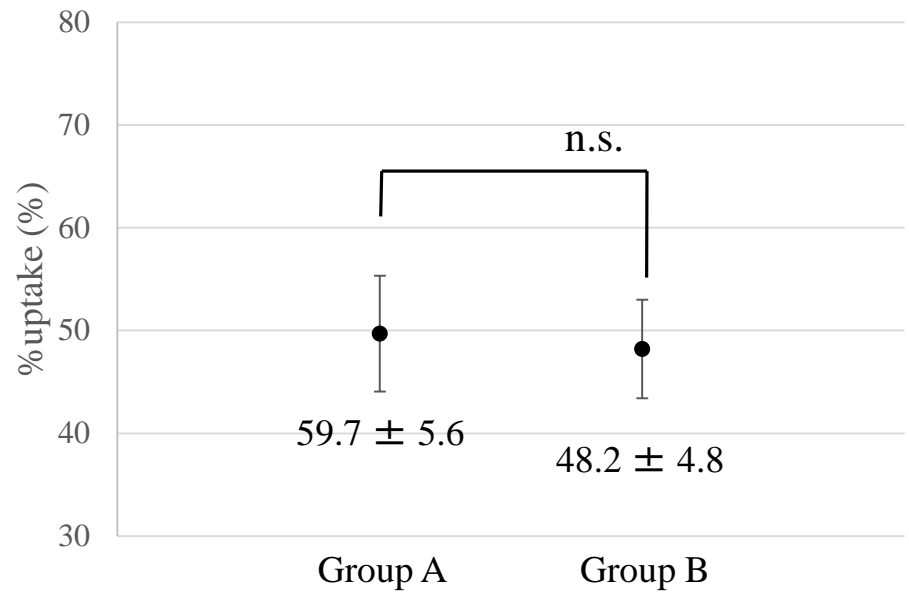
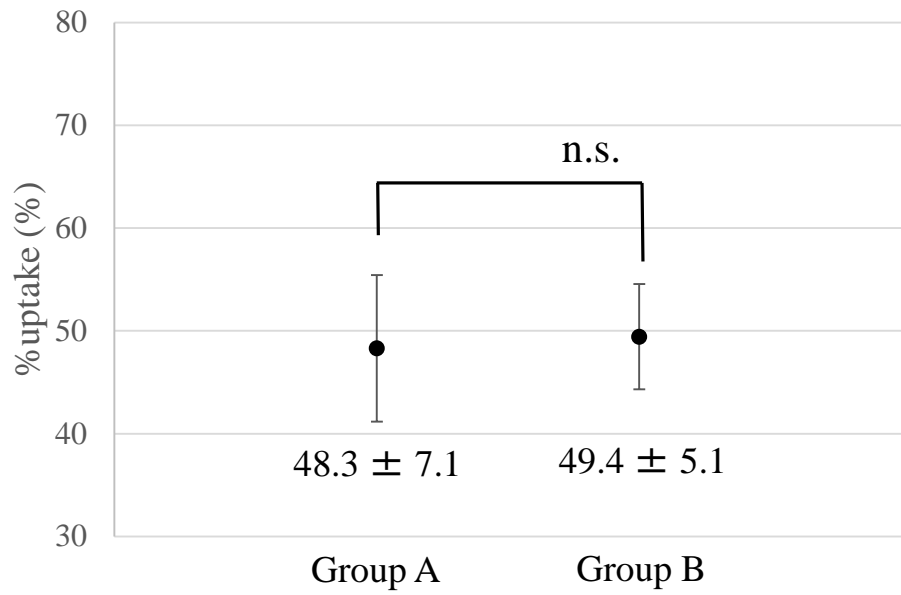


Fig.5

a	b
c	d

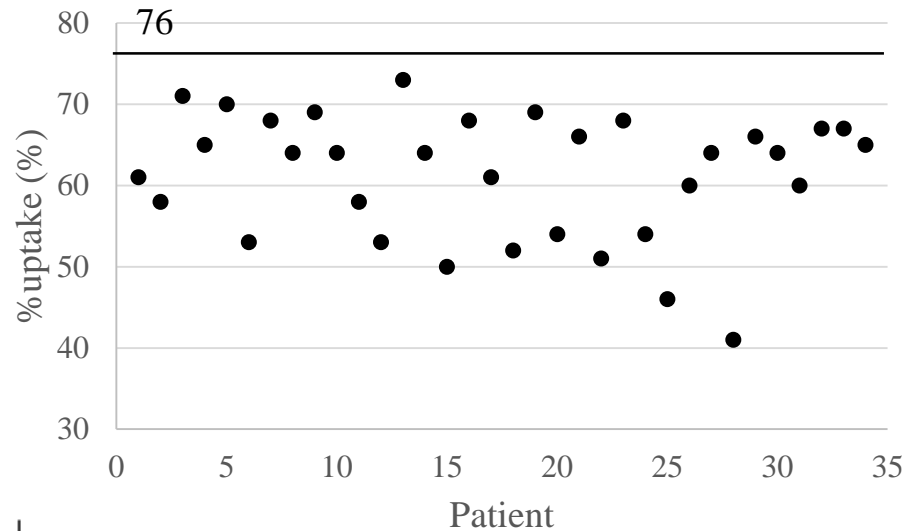
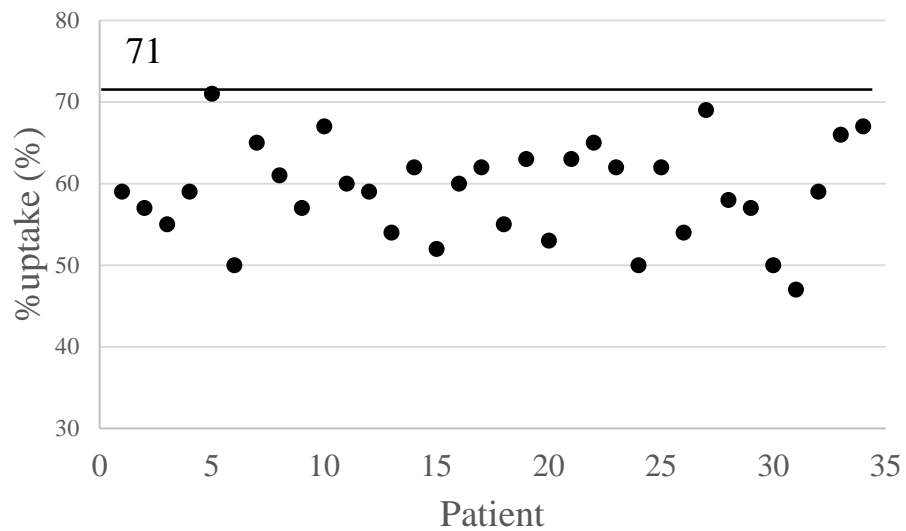
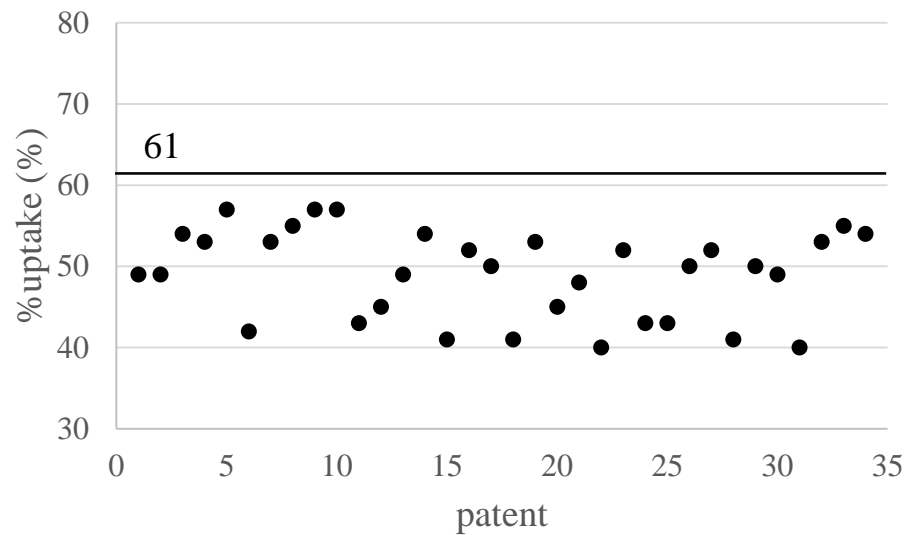
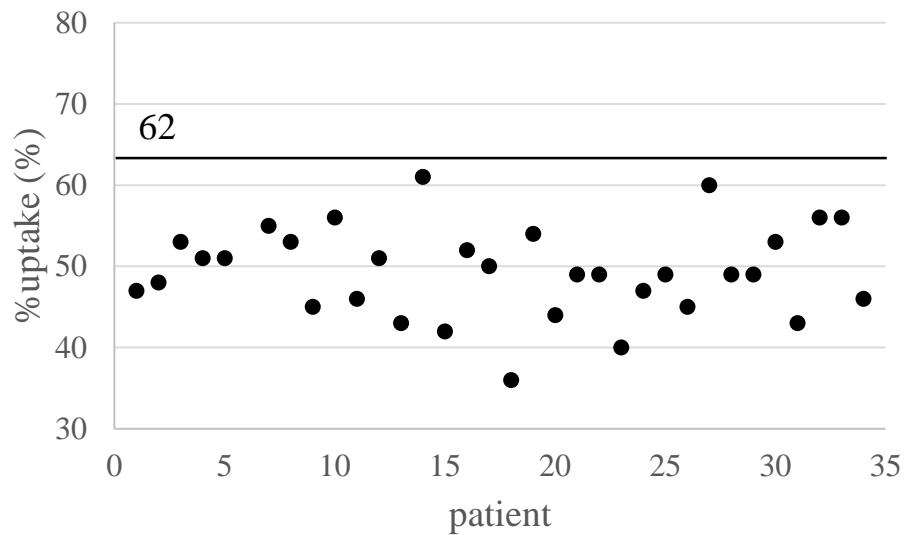


Fig.6

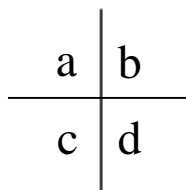


Table.1

	Group A (n = 20)	Group B (n = 14)	Significant difference test
Age (years)	72 ± 6	67 ± 11	n.s.
Male	19 (95.0%)	14 (100%)	n.s.
Height (m)	1.66 ± 0.04	1.63 ± 0.05	n.s.
Body weight (kg)	67.9 ± 8.16	64.0 ± 4.7	n.s.
Body mass index	24.7 ± 2.49	24.1 ± 2.14	n.s.
<b>Coronary risk factors</b>			
Diabetes mellitus	12 (60.0%)	10 (71.4%)	n.s.
Hypertension	13 (65.0%)	11 (73.0%)	n.s.
Hyperlipidemia	7 (35.0%)	13 (92.6%)	p < 0.01
Smoking	4 (20.0%)	8 (57.14%)	p < 0.05

Group A = artifact (attenuation artifacts from the diaphragm) group, Group B = Right coronary artery (RCA) disease group